Photonic crystals

DOI: 10.1002/smll.200800367

Enhanced Fluorescence on a Photonic Crystal Surface Incorporating Nanorod Structures**

*Wei Zhang, Nikhil Ganesh, Patrick C. Mathias, and Brian T. Cunningham**

Fluorescence has long been recognized as an important tool for probing biological structure and function. Development of optically active structures that can enhance fluorescence intensity has gained much attention as a means for detecting fluorescent-tagged analytes at low concentrations for applications in DNA expression analysis and protein diagnostic assays. The majority of structures developed to date for this purpose utilize plasmon resonances of metals to increase the excitation of fluorophores through enhanced near fields,[1–3] to increase the quantum yield by increasing the intrinsic radiative-decay rate of the fluorophores,[4–6] to increase the directional emission,[7–9] or to employ some combination of these processes.[10–14]

Recently, photonic crystals (PCs) have also been used to enhance the emission intensity of organic dyes[15–17] and colloidal quantum dots.[18] Because PC resonators are composed of dielectric materials, they will not quench fluorophores close to their surface by resonant energy transfer,[19] and they can exhibit high Q-factors due to their low absorption loss. Typically comprising a 1D or 2D periodic surface structure formed from a low refractive index (RI) dielectric material that is overcoated with a high-RI thin film, these PCs can be fabricated inexpensively upon plastic substrates over large areas by a nanoreplica molding process[20] and incorporated into the surface of glass slides, microfluidic channels,[21] and microtiter plates.[22] The grating period, grating depth, film thicknesses, and RIs of the materials are chosen in such a way that the PCs can support guided-mode resonances at designated wavelengths,[23–25] where the PCs reflect ≈100% of incident light at the resonant wavelengths, and all other wavelengths are transmitted. Under resonant conditions, excited leaky guided modes are localized in space during their finite lifetimes, which results in the enhancement of the near electric field intensity of the PC structure, and thus enhances the excitation of fluorophores near the PC surface.[26]

Glancing-angle deposition (GLAD)[27–29] is a physical vapor deposition technique in which the angle between the incoming flux and the surface of the substrate is set to be typically less than 15°. When the mobility of atoms is limited, a self-shadowing effect[30,31] during deposition results in a highly porous film, with a structure composed of isolated vertical nanorods. In previous research, we have demonstrated how these nanorod films applied to the surface of label-free PC biosensors increases detection sensitivity by enhancing the available surface area for biochemical binding.[32] In this Communication, we show the enhancement of fluorescence on a PC surface through application of a dielectric nanorod film to the device. We demonstrate enhancement in fluorescence intensity of up to 114 times in comparison to an unpatterned glass slide.

Figure 1a shows the cross section of the PC, which consists of a 1D grating in UV-cured polymer (UVCP) coated with thin films of dense SiO_2 and TiO_2. The layer of SiO_2 with the same RI as the UVCP acts as a spacer layer, preventing the high-electric-field region from exciting background fluorescence in the UVCP. When illuminated with TE polarized light (electric field parallel to the grating lines, ie., the y-axis) at an incident

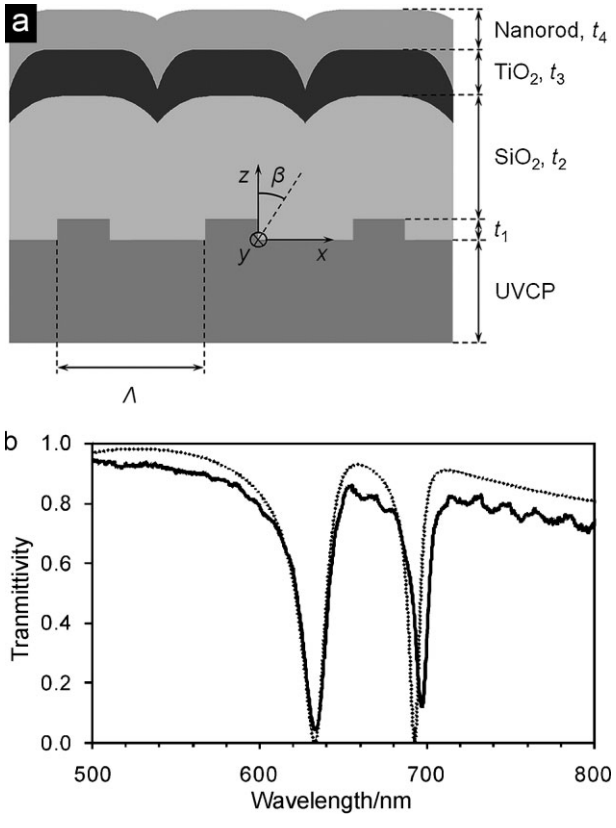

Figure 1. a) Schematic of the cross section of the 1D PC. $\Lambda = 360$ nm is the period of the grating, $t_1 = 60$ nm is the grating depth, $t_3 = 100$ nm is the thickness of the high RI TiO_2 layer and t_4 is the thickness of the nanorod layer. b) Simulated (dotted) and measured (solid) transmission spectra of the PC without nanorod film ($t_4 = 0$ nm) upon illumination with TE polarized light, incidence angle $\beta = 6.0°$.

[*] Prof. B. T. Cunningham, W. Zhang, N. Ganesh, P. C. Mathias
Nano Sensors Group
Micro and Nanotechnology Laboratory
University of Illinois at Urbana-Champaign
208 North Wright Street
Urbana, IL 61801 (USA)
Fax: (+1) 217-244-6375;
E-mail: bcunning@illinois.edu

[**] This work was supported by the National Science Foundation under Grant No. 0427657. Any opinions, findings, and conclusions or recommendations expressed in this material are those of the author(s) and do not necessarily reflect the views of the National Science Foundation. The authors gratefully acknowledge SRU Biosystems for providing financial support for this work. The authors also extend their gratitude to the support staff of the Micro and Nanotechnology Laboratory at the University of Illinois at Urbana-Champaign.

angle $\beta = 6.0^\circ$, the transmission spectrum of PC consists of two resonant dips, one at $\lambda = 633$ nm, which overlaps with the output wavelength of a HeNe laser used to excite Cyanine-5 (Cy5) fluorophore, and a second dip at $\lambda = 694$ nm (Figure 1b).

After PC fabrication (See Experimental Section), the GLAD technique was used to apply nanorod-structured TiO_2 with eight different thicknesses ranging from 25 to 277 nm onto the PC surface by electron-beam deposition (Figure 2a, also see Experimental Section). The self-shadowing effect and limit on surface diffusion in the GLAD technique results in the formation of nanorod structures uniformly coated on the PC surface, as shown in the scanning electron microscopy (SEM) images in Figure 2b.The rod diameter and the spacing between rods are difficult to estimate from the SEM images due to the random structure of the film and the observed degree of rod taper. The RI of the nanorod films that were co-deposited on Si wafers positioned next to the PCs was measured to be $n_{\text{nanorod}} \approx 1.46$ at a wavelength of 633 nm by ellipsometry for all film thicknesses. The reason for the constant RI as a function of film thickness is that the self-shadowing in GLAD causes broadening of some rods but also leads to extinction of others, therefore maintaining a nearly uniform density (determined primarily by the flux incidence angle θ) as the film grows.[33] Since TiO_2 films deposited by evaporation at normal incidence or by sputtering have a RI of $n_{TiO_2} = 2.2$, the nanorod films are estimated to have a porosity of 65%, assuming a linear dependence of RI on porosity.[34–35] Based on the ellipsometry result, a simplified physical model was constructed to make a rough estimate of the surface area available due to the nanorod film. If the nanorod film of thickness t_4 nm is assumed to consist of cylindrical rods with the same diameter, arranged in a square lattice with equal spacing between adjacent rods, a film with 65% porosity is obtained with a rod diameter of $D \approx 30$ nm and a gap of $g \approx 15$ nm between adjacent rods. The extra surface area provided by each rod is the area of the sidewall, which is equal to $\pi D t_4$. The ratio of the total surface area of such a film over that of a flat surface is then given by:

$$areafactor = \frac{\pi D t_4 + (D+g) \times (D+g)}{(D+g) \times (D+g)} = 1 + \frac{30\pi}{45^2} \times t_4 \quad (1)$$

Rigorous coupled-wave analysis (RCWA)[36] simulations were used to study the response of PCs upon external illumination (see Experimental Section). For a PC without nanorod film, the computed transmission spectrum for illumination with incident light ($\beta = 6.0^\circ$, TE polarization, z direction) is shown as the dotted curve in Figure 1b, and is in good agreement with the experimentally measured spectrum, shown as the solid curve. The $\lambda = 633$-nm resonance has a full width at half-maximum (FWHM) of $\Delta\lambda = 19.5$ nm. For PCs with nanorod films, the near electric field intensity E^2 was calculated as a function of nanorod thickness ranging from 0 to 300 nm and the results for 0, 105 and 200 nm are plotted in Figure 3a, b, and d. Note that the most intense near electric field is located in the dense TiO_2 layer, which has the highest RI and decays into the layers above and below.[37]

To compare the emission intensities of fluorophores on PCs with different thickness nanorod films, all PCs were first functionalized with a proprietary polymer consisting of a long, narrow molecular chain with a high density of amine (NH_2) functional groups available along its backbone. For this step, all PCs were incubated with a 1% solution of such amine polymer in water for 26 hours, followed by washing with water. Next, the PCs were immersed in a bifunctional linker, 25% glutaraldehyde ($C_5H_8O_2$, Sigma–Aldrich) in water, for 6 hours, followed by a wash step. The last step of the protocol was to attach a fluorophore molecule to the PC surface. Eight spots of 1 μL of Cy5-conjugated streptavidin (10 μg mL^{-1}; GE healthcare) were hand-spotted onto the PCs using a pipette and allowed to incubate for 30 hours, followed by a wash step. The same protocol was also applied to an unpatterned microscope slide which served as a reference. Since the affinity of the surface chemistry layers is different for different materials, in order to make a comparison the reference slide was previously coated with an 18-nm layer of dense TiO_2 by sputtering. After application of the Cy5-conjugated streptavidin spots, all devices were scanned at 20-μm pixel resolution in a fluorescence scanner (LS 2000, Tecan), equipped with a $\lambda = 633$ nm HeNe laser.

The images of Cy5-conjugated streptavidin spots on all the devices, including the reference slide, are shown in Figure 4a. A line profile of the fluorescence intensity across all devices was taken and is plotted in Figure 4b. After background subtraction, the highest average signal of 11 123 counts within 8 spots was obtained from the PC with 97 nm of nanorod film. This is over 114 times the enhancement when compared to the signal of the reference unpatterned microscope slide, which had an average intensity of 97 counts. As a function of nanorod

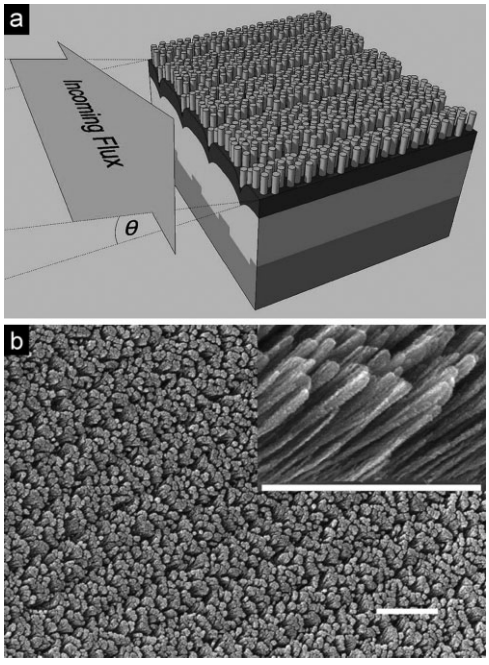

Figure 2. a) Schematic of the GLAD setup. $\theta = 5.0^\circ$ is the angle between the incoming flux and the PC surface. b) SEM images of the top view and side view (inset) of a nanorod-coated PC with 277 nm of nanorod TiO_2. Scale bars = 500 nm.

thickness, the fluorescence intensity increases gradually from 0 nm (1 231 counts) up to 97 nm (11 123 counts), then starts to decrease slowly until it reaches a plateau at about 238 nm (6 955 counts). At the maximum nanorod thickness of all the PCs, 277 nm, the average intensity is 7 290 counts.

The overall enhancement of fluorescence intensity comes from a combination of enhanced near-electric fields due to the resonance effect and enhanced surface area due to the presence of nanorod structure. Assuming the fluorophores are uniformly distributed within the nanorod films, we expect the product of average E^2 within the nanorod film (calculated as a function of nanorod thickness using RCWA and shown as the dotted curve in Figure 5a) and the area factor (given by Equation 1) would be a reasonable figure of merit describing how the total enhancement changes with nanorod thickness. In order to compare with experimental fluorescence intensity, this product is calculated as a function of nanorod thickness and normalized to the experimentally measured fluorescence intensity of the PC without nanorod coating (1 231 counts). The result is plotted as the curve in Figure 5b and we see an excellent agreement with the measured intensities shown as the diamonds.

Further analysis of the relation between fluorescence intensity and nanorod thickness reveals that the trend shown in Figure 5b may be explained by three effects introduced by the nanorod film, which here we refer to as surface area, Q-factor, and near-field distribution. The first effect of surface area is explained by Equation 1: the total surface area of nanorod film increases linearly with thickness, assuming the simplified model mentioned above. In reality, as the nanorod thickness increases, it becomes more and more difficult for the surface chemistry molecules and fluorophores to diffuse into the bottom regions of the film and fully utilize the extra surface area. Furthermore, the observed degree of taper (shown in the inset of Figure 2b) in the nanorod structure also increases with thickness, which could make the diffusion of molecules even more difficult. These factors might explain the deviation of experimental data from the predicted curve above 200 nm in Figure 5b.

The second effect of Q-factor is related to the fact that the introduction of nanorod film changes the RI of the superstrate of PC, thus changing the quality of the resonance and the overall intensity of the near fields. As shown in Figure 5a for both the calculated (solid curve) and measured (diamonds) data, the Q-factor of the 633 nm resonance increases as nanorod thickness increases until reaching a maximum at about 105 nm. Thereafter the Q-factor starts decreasing until it reaches a local minimum at about 200-nm nanorod thickness, at which point the trend starts to reverse again. This relation of Q-factor (therefore the overall intensity of near fields) and the nanorod thickness is confirmed by the calculated field-intensity distributions shown in Figure 3, that is, PC coated with 105 nm of nanorod has much higher E^2 compared to PCs with 0 and 200 nm (both thicknesses are of local minima of the Q-factor curve in Figure 5a) nanorod films.

The last effect, near-field distribution, refers to the fact that fluorophores within the nanorod film have a chance to interact with additional regions of the near-field resonant mode distribution, since the nanorod structure extends the surface area for binding into a 3D volume. As shown in Figure 3, although the overall intensity of the near electric field changes with nanorod thickness, the spatial distribution remains about the same. The solid curve in Figure 3c shows the computed average E^2 across the x-direction plotted as a function of the vertical dimension, z, in Figure 3b. The most intense near electric field is positioned in the high-RI layer of dense TiO_2, above which E^2 decreases with z. Since E^2 is above unity (shown as the dotted line in Figure 3c), which is the normalized incident-light intensity, fluorophores in this region will have enhanced emission intensity, and increasing the nanorod thickness will increase the total fluorescence intensity. Once the nanorod thickness reaches about 208 nm (z = 671 nm), the film enters the node of the standing-wave interference pattern above the PC. Further increase of the nanorod thickness will not be very effective in further enhancing the total fluorescence intensity since E^2 in this region is below unit intensity. The combined effect of Q-factor and near-field distribution is represented by the average E^2 within the nanorod film, plotted as the dotted curve in Figure 5a.

Such a fluorescence-enhancement scheme combining a PC structure and a high surface-area coating with nanometer-scale dimensions can be invaluable to the future design of devices. Since the nanorod structure extends the available surface area into a 3D volume, the whole volume, instead of the very first layer of the near fields, can be used to enhance the excitation of fluorophores. The Q-factor of the PC reported in this study is relatively low ($Q \approx 33$) and future work will focus on combing PC design of high Q-factor (as high as $Q \approx 2000$ demonstrated[38]) with high surface-area nanorod structures to achieve even higher fluorescence-intensity enhancement.

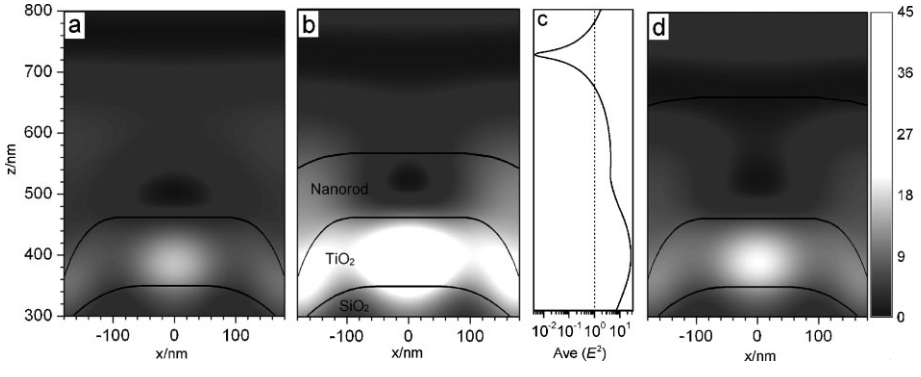

Figure 3. Calculated near electric field intensity E^2 for PCs with a) 0 nm, b) 105 nm, and d) 200 nm of nanorod films using RCWA. c) Average E^2 along x-direction as a function of vertical dimension, z, in (b).

Experimental Section

Photonic crystal fabrication process: The 1D PC structure was fabricated by a cost-effective nanoreplica molding process.[20] Electron-beam

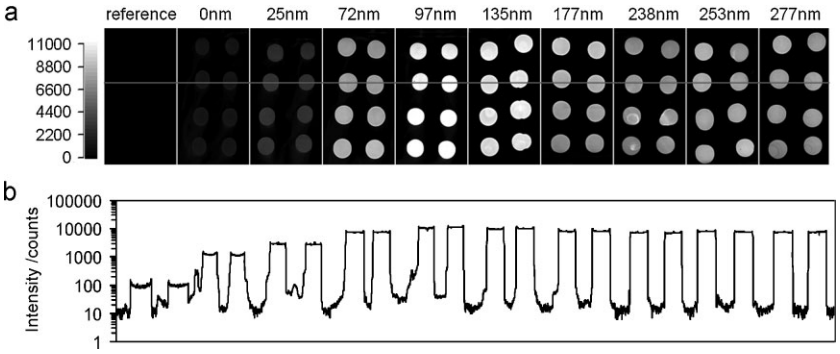

Figure 4. a) Images of Cy5-conjugated streptavidin spots on a reference slide (unpatterned glass slide coated with 18 nm of sputtered TiO_2) and PCs with different nanorod thicknesses. b) Intensity plot of the horizontal line in (a).

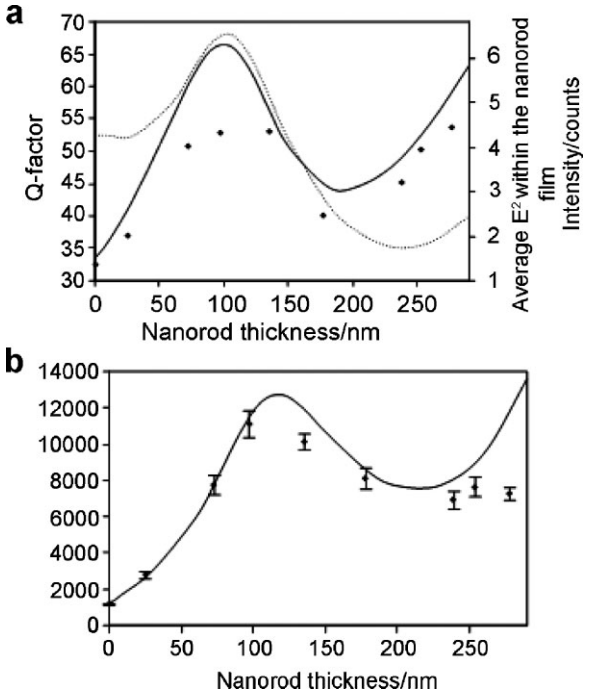

Figure 5. a) Measured (diamonds) and calculated (solid curve) Q-factor of the 633-nm resonance and calculated average of the near-electric-field intensity E^2 (dotted curve) within the nanorod films for PCs with different nanorod thicknesses. b) Measured fluorescence intensities (diamonds, with error bar showing $N = 8$) and simulated intensities (curve) as a function of nanorod thickness.

lithography was used to define, on a Si "master" wafer, the negative image of the desired surface structure pattern, in this case a linear grating with a period of $\Lambda = 360$ nm and a grating depth of $t_1 = 60$ nm, as shown in Figure 1a. A thin layer of liquid UV-curable polymer was then sandwiched between a flexible polyester substrate and the master wafer. After the UV-curable polymer was cured ($n_{UVCP} = 1.46$), the polyester sheet with the grating structure was peeled away from the master wafer. A layer of SiO_2 ($n_{SiO_2} = 1.46$) was deposited onto the structure by electron-beam deposition and a layer of TiO_2 ($n_{TiO_2} = 2.25$, $t_3 = 100$ nm) was sputtered onto the device surface as the last step of fabrication. The completed device was then mounted onto a microscope slide using an optical adhesive.

Glancing angle deposition: GLAD was performed in an electron-beam deposition system (Temescal) with a base pressure of 1.0×10^{-6} Torr and a deposition rate of 10 Å s^{-1}. The angle between the incoming flux of evaporated material and the PC surface was set to be $\theta = 5.0^\circ$, as shown in Figure 2a. To minimize the shadowing effect between grating lines, the incoming flux was chosen to be parallel to the grating sidewalls and no substrate rotation was used during deposition. Also, no substrate heating was used, in order to minimize the mobility of the atoms. Nanorod films with eight different thicknesses ranging from 25 to 277 nm were deposited upon PCs that were previously prepared with a dense layer of TiO_2 applied by sputtering, as described above.

Rigorous coupled-wave analysis simulations: Theoretical calculations were made using commercial software (DiffractMOD, Rsoft Design Group) utilizing the RCWA algorithm. A model of the PC structure with the dimensions given in Figure 1a was made. Periodic boundary conditions were applied to the x extent, and y was invariant. For PCs with nanorod films, since the feature size of the nanorod structure was much smaller than the wavelength of light used in this study, Mie- and Rayleigh-scattering could be neglected[39] and local "hot spots" of high electric field due to the dielectric rod structures were not expected as in the case of metallic nanostructures. Therefore, the nanorod film was considered to be a uniform layer without any internal structure in the simulation. The RI of the nanorod layer was set to be $n_{nanorod} = 1.46$ for all nanorod thickneses. All materials were assumed to be lossless.

Keywords:

fluorescence · nanorods · photonic crystals · TiO_2 films

[1] T. Hayakawa, S. T. Selvan, M. Nogami, *Appl. Phys. Lett.* **1999**, *74*, 1513.
[2] S. T. Selvan, T. Hayakawa, M. Nogami, *J. Phys. Chem. B* **1999**, *103*, 7064.
[3] Y. J. Hung, I. I. Smolyaninov, C. C. Davis, H. C. Wu, *Opt. Express* **2006**, *14*, 10825.
[4] W. L. Barnes, *J. Mod. Optic.* **1998**, *45*, 661.
[5] J. R. Lakowicz, *Anal. Biochem.* **2001**, *298*, 1.
[6] J. R. Lakowicz, Y. B. Shen, S. D'Auria, J. Malicka, J. Y. Fang, Z. Gryczynski, I. Gryczynski, *Anal. Biochem.* **2002**, *301*, 261.
[7] K. Aslan, I. Gryczynski, J. Malicka, E. Matveeva, J. R. Lakowicz, C. D. Geddes, *Curr. Opin. Biotechnol.* **2005**, *16*, 55.
[8] J. R. Lakowicz, *Plasmonics* **2006**, *1*, 5.
[9] K. Aslan, S. N. Malyn, C. D. Geddes, *J. Fluoresc.* **2007**, *17*, 7.
[10] J. Enderlein, *Appl. Phys. Lett.* **2002**, *80*, 315.
[11] Y. D. Liu, S. Blair, *Opt. Lett.* **2003**, *28*, 507.
[12] Y. Fu, J. R. Lakowicz, *Anal. Chem.* **2006**, *78*, 6238.
[13] Y. Fu, J. R. Lakowicz, *J. Phys. Chem. B* **2006**, *110*, 22557.
[14] Y. Chen, K. Munechika, D. S. Ginger, *Nano Lett.* **2007**, *7*, 690.
[15] W. Budach, D. Neuschafer, C. Wanke, S. D. Chibout, *Anal. Chem.* **2003**, *75*, 2571.

[16] D. Neuschafer, W. Budach, C. Wanke, S. D. Chibout, *Biosens. Bioelectron.* **2003**, *18*, 489.
[17] P. C. Mathias, N. Ganesh, L. L. Chan, B. T. Cunningham, *Appl. Opt.* **2007**, *46*, 2351.
[18] N. Ganesh, W. Zhang, P. C. Mathias, E. Chow, J. A. N. T. Soares, V. Malyarchuk, A. D. Smith, B. T. Cunningham, *Nat. Nanotechnol.* **2007**, *2*, 515.
[19] N. Ganesh, P. C. Mathias, W. Zhang, B. T. Cunningham, *J. Appl. Phys.* **2008**, *103*, 083104.
[20] N. Ganesh, B. T. Cunningham, *Appl. Phys. Lett.* **2006**, *88*, 071110.
[21] C. J. Choi, B. T. Cunningham, *Lab Chip* **2006**, *6*, 1373.
[22] B. T. Cunningham, P. Li, S. Schulz, B. Lin, C. Baird, J. Gerstenmaier, C. Genick, F. Wang, E. Fine, L. Laing, *J. Biomol. Screening* **2004**, *9*, 481.
[23] S. S. Wang, R. Magnusson, J. S. Bagby, M. G. Moharam, *J. Opt. Soc. Am. A* **1990**, *7*, 1470.
[24] R. Magnusson, S. S. Wang, *Appl. Phys. Lett.* **1992**, *61*, 1022.
[25] S. S. Wang, R. Magnusson, *Appl. Opt.* **1993**, *32*, 2606.
[26] C. Y. Wei, S. J. Liu, D. G. Deng, J. Shen, J. D. Shao, Z. X. Fan, *Opt. Lett.* **2006**, *31*, 1223.
[27] J. G. W. van der Waterbeemd, G. W. van Oosterhout, *Philips Res. Rep.* **1967**, *22*, 375.
[28] K. Robbie, L. J. Friedrich, S. K. Dew, T. Smy, M. Brett, *J. Vac. Sci. Technol. A* **1995**, *13*, 1032.
[29] L. Abelmann, C. Lodder, *Thin Solid Films* **1997**, *305*, 1.
[30] H. Konig, G. Helwig, *Optik* **1950**, *6*, 111.
[31] L. Holland, *J. Opt. Soc. Am.* **1953**, *43*, 376.
[32] W. Zhang, N. Ganesh, I. D. Block, B. T. Cunningham, *Sens. Act. B* **2008**, *131*, 279.
[33] B. Dick, M. J. Brett, T. Smy, *J. Vac. Sci. Technol. B* **2003**, *21*, 23.
[34] D. J. Taylor, P. F. Fleig, S. L. Hietala, *Thin Solid Films* **1998**, *332*, 257.
[35] J. Q. Xi, J. K. Kim, E. F. Schubert, D. Ye, T.-M. Lu, S.-Y. Lin, *Optics Letters* **2006**, *31*, 601.
[36] M. G. Moharam, T. K. Gaylord, *J. Opt. Soc. Am.* **1981**, *71*, 811.
[37] Y. Ding, R. Magnusson, *Opt. Express* **2004**, *12*, 1885.
[38] A. S. P. Chang, S. Bai, H. Tan, W. Wu, Z. Yu, S. Y. Chou, presented at LEOS 2002, Glasgow, Scotland, 2002.
[39] J. Q. Xi, M. F. Schubert, J. K. Kim, E. F. Schubert, M. F. Chen, S. Y. Lin, W. Liu, J. A. Smart, *Nat. Photonics* **2007**, *1*, 176.

Received: March 13, 2008
Revised: May 22, 2008

